Forecasting Tropical Cyclones in the Western North Pacific Basin Using the NCEP Operational HWRF: Real-Time Implementation in 2012

VIJAY TALLAPRAGADA

NOAA/NWS/NCEP/Environmental Modeling Center, College Park, Maryland

CHANH KIEU, SAMUEL TRAHAN, AND ZHAN ZHANG

NOAA/NWS/NCEP/Environmental Modeling Center, College Park, and I.M. Systems Group, Rockville, Maryland

QINGFU LIU

NOAA/NWS/NCEP/Environmental Modeling Center, College Park, Maryland

WEIGUO WANG, MINGJING TONG, AND BANGLIN ZHANG

NOAA/NWS/NCEP/Environmental Modeling Center, College Park, and I.M. Systems Group, Rockville, Maryland

BRIAN STRAHL

Joint Typhoon Warning Center, Pearl Harbor, Hawaii

(Manuscript received 14 October 2014, in final form 21 May 2015)

ABSTRACT

This study documents the recent efforts of the hurricane modeling team at the National Centers for Environmental Prediction's (NCEP) Environmental Modeling Center (EMC) in implementing the operational Hurricane Weather Research and Forecasting Model (HWRF) for real-time tropical cyclone (TC) forecast guidance in the western North Pacific basin (WPAC) from May to December 2012 in support of the operational forecasters at the Joint Typhoon Warning Center (JTWC). Evaluation of model performance for the WPAC in 2012 reveals that the model has promising skill with the 3-, 4-, and 5-day track errors being 125, 220, and 290 nautical miles (n mi; 1 n mi = 1.852 km), respectively. Intensity forecasts also show good performance, with the most significant intensity error reduction achieved during the first 24 h. Stratification of the track and intensity forecast errors based on storm initial intensity reveals that HWRF tends to underestimate storm intensity for weak storms and overestimate storm intensity for strong storms. Further analysis of the horizontal distribution of track and intensity forecast errors over the WPAC suggests that HWRF possesses a systematic negative intensity bias, slower movement, and a rightward bias in the lower latitudes. At higher latitudes near the East China Sea, HWRF shows a positive intensity bias and faster storm movement. This appears to be related to underestimation of the dominant large-scale system associated with the western Pacific subtropical high, which renders weaker steering flows in this basin.

1. Introduction

Previous studies have shown that forecasts for tropical cyclones (TCs) in the western North Pacific basin (WPAC) generally possess a high degree of uncertainty as a result of the complex topography, intricate monsoon influences, or multiple vortex interactions in this region (Chang 1982; Lin et al. 1999; Payne et al. 2007; Kehoe et al. 2007; Tien et al. 2012). The complicated behavior of the TC tracks and intensity can be seen most clearly in terms of frequent irregular track patterns in the WPAC such as tracks with multiple loops or sharp changes in storm movement. For example, Typhoon Tembin (2012) made a complete loop back to the east before resuming a northward track east of Taiwan,

Corresponding author address: Dr. Vijay Tallapragada, NOAA/NWS/NCEP/Environmental Modeling Center, 5830 University Research Court, College Park, MD 20740.
E-mail: vijay.tallapragada@noaa.gov

DOI: 10.1175/WAF-D-14-00138.1

possibly under the influence of the nearby Typhoon Bolaven (2012; cf. Fig. 4, described in greater detail below). These complications could partially explain the higher track and intensity forecast errors in the WPAC as compared to those in the North Atlantic basin (NATL) or the eastern North Pacific basin (EPAC; see, e.g., Carr and Elsberry 2000; Payne et al. 2007; Brown et al. 2010; Cangialosi and Franklin 2013; Evans and Falvey 2013).

The large uncertainties in TC track and intensity forecasts in the WPAC render TC forecasting in this ocean basin challenging. In addition to model internal deficiencies, a number of external factors that can also impact the forecast skill of regional numerical models in this area include the errors of the global models in WPAC that provide initial and boundary conditions for regional models, the scarcity of real-time flight reconnaissance observations, or complicated large-scale interactions (e.g., Carr and Elsberry 1998, 2000; Kehoe et al. 2007). For instance, underrepresentation of the vortex-scale circulation in the NCEP Global Forecast System (GFS) and lack of real-time inner-core observations within the TC circulation often result in an improper vortex initialization for any regional TC models that are directly driven by the GFS analysis. A model vortex initialized directly from the GFS often shows a very weak storm, typically about 30% weaker in terms of the maximum 10-m wind and even more so during the mature stage of a TC, and is often exaggerated in the WPAC because of statistically stronger TCs in this basin (see, e.g., Kurihara et al. 1998; Bender et al. 2007; Nolan et al. 2009; Gopalakrishnan et al. 2012b; Tien et al. 2013). All of these factors generate large uncertainties in the TC track and intensity forecasts in the WPAC, where the official track and intensity errors are usually larger than those in NATL and EPAC. For instance, in 2012, National Hurricane Center (NHC) mean official track forecast errors for the NATL were around 40, 69, 101, 143, and 194 nautical miles (n mi; 1 n mi = 1.852 km) at 1–5-day forecast lead times, respectively (Cangialosi and Franklin 2013), whereas the corresponding JTWC mean official track forecasts for the WPAC were 48, 87, 121, 160 and 218 n mi at 1–5-day forecast lead times, respectively (Evans and Falvey 2013), indicating about 20% larger errors in the WPAC compared to NATL.

Given the high degree of uncertainty of TC forecasts in this ocean basin, consensus of multiple models or ensemble forecasts is an optimal choice for improving the operational forecast skill as these ensemble approaches could take into account the strengths and weaknesses of each individual model (e.g., Evans and Falvey 2013). In an attempt to support operational forecasters at the JTWC, the hurricane modeling team at NCEP's Environmental Modeling Center (EMC) has recently been requested to provide experimental real-time TC forecast guidance for the WPAC using the operational Hurricane Weather Research and Forecasting Model (HWRF) that was designed for providing real-time TC guidance to the NHC area of operations (NATL and EPAC). The inspiration for this experimental real-time setup came from the successful implementation of the advanced high-resolution triple-nested HWRF for the NATL and EPAC for the 2012 hurricane season (Tallapragada et al. 2014) and support from the National Oceanic and Atmospheric Administration's (NOAA) Hurricane Forecast Improvement Project (HFIP; Gall et al. 2013). In this paper and in Tallapragada et al. (2015, manuscript submitted to *Wea. Forecasting*, hereafter TWAF), we document NCEP/EMC's efforts in implementing the real-time TC forecasting system for the WPAC. This paper is focused on describing HWRF's performance for the WPAC in 2012, with an objective of identifying the strengths and weaknesses of HWRF in this ocean region as compared to other operational regional models used by JTWC. Another objective is to gain some insights into the specific behaviors of HWRF, and to better understand the characteristics of TCs in the WPAC region. The outcomes from the evaluation of real-time experiments in the WPAC are also anticipated to help make further improvements to HWRF for more skillful operational forecasts in future years. TWAF will document the upgrades implemented into HWRF for real-time 2013 WPAC forecast experiments, where significantly lower intensity errors are obtained.

This paper is organized as follows. In the next section, an overview of the 2012 operational HWRF and the real-time setup for the WPAC are provided. Section 3 presents detailed forecast verifications of HWRF for the WPAC. Concluding remarks and future work are given in the final section.

2. Real-time configuration for 2012 operational HWRF

a. *The 2012 HWRF implementation at NCEP for the North Atlantic and eastern North Pacific basins*

The operational HWRF is a high-resolution hurricane model with triple-nest capability based on the community version of the Weather Research and Forecasting Model, version 3.4a–Nonhydrostatic Mesoscale Model (WRF-NMM) (Janjic 2003; Janjic et al. 2001, 2010; Gopalakrishnan et al. 2012a; Tallapragada et al. 2012). The model consisted of three nested domains with horizontal resolutions of 27, 9, and 3 km; the outermost

TABLE 1. List of HWRF configurations for the 2012 WPAC real-time experiment.

Scheme	Notes
Model horizontal resolution	27, 9, and 3 km (E grid)
Dynamics core	WRF-NMM, version 3.4a
Model domain	216 × 432 (27 km), 88 × 170 (9 km), and 154 × 272 (3 km)
No. of vertical hybrid levels	43
Cumulus parameterization (shallow and deep)	Simplified Arakawa–Schubert (27- and 9-km domains only)
Microphysics parameterization	Ferrier
Boundary layer	Modified GFS PBL scheme
Surface physics	Improved GFDL
Radiation	GFDL short- and longwave schemes
Lateral boundary conditions	GFS updated every 6 h
Frequency of physics calls	3 min

domain is fixed in time for each forecast cycle while the telescopic moveable 9- and 3-km domains follow the predicted storm center.

HWRF domains were configured in rotated latitude–longitude coordinates with 43 sigma vertical levels defined as follows (Arakawa and Lamb 1977; Janjic et al. 2010):

$$\sigma = \frac{\pi - \pi_t}{\pi_s - \pi_t},$$

where π is the hydrostatic pressure at each vertical level and $\pi_s(\pi_t)$ is the pressure at the surface (top of the model). The model domains were storm centric with 216 × 432 grid points for the 27-km parent grid; 88 × 170 grid points for the 9-km intermediate grid; and 154 × 272 grid points for the 3-km innermost domain in the (x, y) directions, respectively. Model physics tailored for hurricane[1] forecasting included the modified GFS PBL scheme (Gopalakrishnan et al. 2012b), an improved Geophysical Fluid Dynamics Laboratory (GFDL) surface physics (Kwon et al. 2009), the Ferrier microphysics parameterization scheme modified for TC applications (Ferrier 1994), the GFDL radiative schemes for both short- and longwave parameterization, and implementation of the new GFS simplified Arakawa–Schubert scheme for both shallow and deep convection parameterization (Han and Pan 2011); see Table 1 for the details of the models' configuration and physics. The model physics was called every 3 min (except for the radiation parameterization, which had a 30-min time step) with explicit representation of convection in the innermost 3-km domain.

[1] The words hurricane and tropical cyclone are used interchangeably throughout the manuscript.

In addition to the hurricane-specific physics, HWRF employed a versatile vortex initialization procedure for the 3-km-resolution grid, with improved interpolation algorithms, and storm size and intensity correction procedures (Liu et al. 2012). Assimilation of the observational data in HWRF was based on the community Gridpoint Statistical Interpolation analysis system, version 3.4 (GSI V3.4; see Kleist et al. 2011). The HWRF system also has an ocean component, based on the Princeton Ocean Model (POM) developed in collaboration with the University of Rhode Island (Yablonsky et al. 2015; Gopalakrishnan et al. 2012a) but this coupled configuration was not operated in the real-time experiments in the WPAC during 2012. A more detailed description of the GSI and ocean coupling can be found in Tallapragada et al. (2014).

b. *HWRF implementation for the western North Pacific basin*

Real-time experiments for the WPAC are configured using the same 2012 operational HWRF (Tallapragada et al. 2012) version implemented at NCEP for the NATL and EPAC, except for the ocean component. HWRF was run in an uncoupled mode for WPAC in 2012 because of the lack of regional ocean model capability for this basin at that time. These experiments were started on 1 May 2012 and continued through the end of the year, run for every WPAC storm, from depression stage through dissipation, four cycles a day at every 6-h interval, using dedicated resources on the NOAA Research and Development (RD) supercomputers (Jet systems) provided by HFIP. Robust automation tools and dedicated reservations were employed to ensure on-time delivery of the forecast products to JTWC. A separate communication channel was used to get real-time storm location, intensity, and structure information (known as tcvitals) from JTWC and upload track and intensity forecasts directly to the Automated Tropical Cyclone Forecasting System (ATCF; Sampson and Schrader 2000) database maintained by the U.S. Navy. Because of the developmental constraints at NCEP/EMC, the fiscal-year (FY) 2012 version of HWRF was not finalized until May 2012. Therefore, the real-time implementation of HWRF for the WPAC was not started until 1 May 2012, and it was maintained for the rest of the year.

Implementation of HWRF for the WPAC required addressing a number of technical issues and customizing several components of the modeling system including removing the artificial boundary limit so that the domain selection procedure is unified for all oceanic basins in the Northern Hemisphere (Liu et al. 2012; Gopalakrishnan et al. 2012a). The vortex initialization procedure originally designed for the NATL and EPAC has also been revised to work in all ocean basins including WPAC and the north Indian Ocean (NIO).

The experimental real-time setup for HWRF in the WPAC followed the same procedures used by NCEP Central Operations (NCO) for the NATL and EPAC. HWRF was initiated when tcvitals data were made available by JTWC for each synoptic cycle at 6-h intervals for each individual storm in the WPAC present at that time. This procedure for each storm started when JTWC identified an area of interest for potential cyclogenesis (INVEST) and was continued through the end of the life cycle of the storm (usually through dissipation over land or by becoming extratropical). HWRF was initialized with the NCEP GFS operational analysis at T574L64 resolution (~27-km horizontal resolution).[2] Lateral boundary conditions for the outer domain were taken from the GFS spectral forecasts at every 6-h interval through the 126-h period.

Real-time forecasts from HWRF were made available for all WPAC TCs during 2012 starting with Typhoon Sanvu (03W) in May 2012 to the last Typhoon Wukong (27W) in December 2012. A complete list of each individual forecast cycle for the 2012 WPAC and corresponding forecast products can also be accessed from HWRF's official website (http://www.emc.ncep.noaa.gov/HWRF/WestPacific/RT_WPAC_FY12).

3. Verification of real-time HWRF forecasts for the western North Pacific basin

For verification of the model forecasts, the final version of the postseason best-track data (bdecks) provided by JTWC were used exclusively, along with the model-generated tracker output in ATCF format (adecks). These datasets provide necessary information including location of the storm center (latitude–longitude); 10-m maximum wind (VMAX); minimum sea level pressure (PMIN); radius of maximum wind (RMW); and storm radii at 34-, 50-, and 64-kt thresholds from observations and model output at every 6-h interval. While there are significant uncertainties in estimating the track, intensity, and different radius information (Landsea and Franklin 2013; Torn and Snyder 2012), the goal of this study is to evaluate the performance of the operational HWRF in comparison to other real-time global and regional model guidance received by JTWC, and to benchmark these metrics for evaluating future upgrades. Because the verification for HWRF is relative to other dynamical models, it is expected that the observational errors should have secondary impacts to the relative performance of HWRF as compared to other models.

To quantify for the subsequent statistics and associated uncertainties, 95% confidence intervals are displayed along with the errors at each forecast lead time. The error bars provided in all of the statistics shown in this paper are obtained from the statistics of forecast errors at each lead time and given by 1.96(std)/sqrt(ncase), where std is the standard deviation and ncase is the number of cases verified at each forecast lead time. Overlap of the error bars thus signifies that the improvement is not statistically significant at $P < 0.05$ by the standard unpaired Student's t test (assuming a Gaussian distribution of the data). Otherwise, the difference between any pair of the models is considered statistically significant. A caveat for the underlying Gaussian assumption is that autocorrelation and variance inflation factors in the dataset will not be taken into account, which could lead to larger error bars since the effective sample size will be much smaller.

a. Track forecast verification

To demonstrate the overall performance of HWRF in the WPAC, Fig. 1 shows homogeneous verification of the HWRF forecasts in terms of track forecast errors, and track-relative (along track and cross track) errors during the experimental period in 2012. These verifications are relative to two other operational regional models run at the U.S. Navy's Fleet Numerical Meteorology and Oceanography Center (FNMOC) including the U.S. Navy's version of the GFDL model (GFDN; Dickerman 2006) run with Navy Operational Global Atmospheric Prediction System (NOGAPS; Hogan and Rosmond 1991) global model input, and the experimental Coupled Ocean–Atmosphere Mesoscale Prediction System for Tropical Cyclones (COAMPS-TC; Doyle et al. 2011) model. The NCEP GFS global forecasts [also known in the past as Aviation Ontime (AVNO)] are also included as a reference, which exhibited significantly lower track errors at all forecast lead times compared to the regional models and JTWC Official (hereafter referred to as simply JTWC) forecasts. One can notice in Fig. 1 that of the three regional models, HWRF has better track forecast performance at all forecast lead times up to 4 days at 95% confidence interval. HWRF's 1–3-day track forecast errors are closer to the AVNO forecasts compared to the other regional models. At lead times longer than 3 days, the HWRF track forecast degrades gradually with respect to the AVNO forecasts with the 4- and 5-day track errors of about 200 and 290 n mi, respectively. Although

[2] Documentation for the GFS's most updated products and implementation is available online (http://www.emc.ncep.noaa.gov/GFS/doc.php).

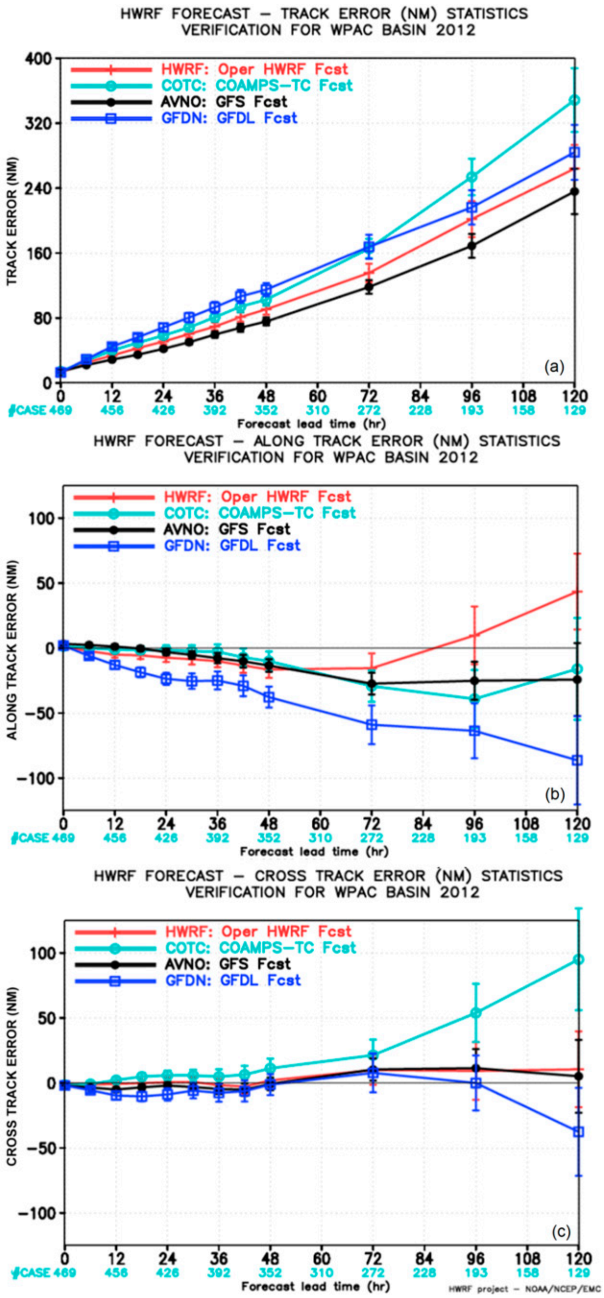

FIG. 1. Verification of the (a) mean absolute track errors, (b) along-track errors, and (c) cross-track errors (n mi) during 2012 in the WPAC for HWRF (red), COAMPS-TC (cyan), AVNO (black), and GFDN (blue). The number below the x axis denotes the number of cases (cycles) at the end of the real-time experiments. The error bars denote the 95% confidence interval.

HWRF errors are still the smallest among the other regional models, we notice that the 4- and 5-day track errors are significantly higher than those in the NATL and EPAC, which are about 180 and 200 n mi, respectively (Tallapragada et al. 2012). This could be attributed to the general lower predictability in the WPAC as previously reported (Pike and Neumann 1987; Payne et al. 2007; Kehoe et al. 2007). Of specific interest is that HWRF appears to possess faster translational speed than the observed tracks at days 4 and 5, as shown in the along-track statistics (Fig. 1b), whereas the cross-track errors seem to be somewhat neutral. Note that although other models have a continued trend in the negative along-track errors at all lead times, the along-track errors in the HWRF become positive at the end of the 5-day lead time.

Unlike the along-track errors, it is of interest to observe that the cross-track errors generally show no systematic left or right bias with the cross-track errors being close to zero (Fig. 1c). On average, the cross-track systematic errors account for less than 10% of the total track errors at all forecast lead times. However, such small cross-track error statistics are due to the cancellation between the right- and left-track errors from different cycles. To analyze the distribution of the track errors over the WPAC region, Fig. 2 shows the 24- and 48-h track forecast errors with respect to the storm initial locations. Here, the along- and cross-track errors are displayed as vectors with the convention that arrows pointing to the northeast indicate faster-moving storms with right bias while those pointing to the southwest denote slower-moving storms with left bias relative to the best track. The magnitudes of these arrows indicate the magnitudes of the absolute track errors. Essentially, Fig. 2 provides information about the geographical distribution of the track errors at 24 and 48 h, given the storm initial locations. The dependence of the storm-track forecast errors on the storm initial location is expected, because the model storms inherit specific environmental properties near their initial positions. Therefore, the storm initial locations could provide us with some information about the track and intensity errors over the next 48 h. Since the dependence of the storm tracks on the storm initial locations tends to decrease quickly with forecast lead times, we will limit the analysis of this dependence only up to 48-h lead time.

Masked from seasonally averaged cross-track error statistics shown in Fig. 1, HWRF exhibits a dominantly left bias in the high-latitude region, while it appears to possess a right bias at the lower latitudes. Along with this division of the cross-track errors with latitudes, HWRF also shows a tendency toward slower translational speeds between 14° and 25°N in the East China Sea, resulting in a somewhat counterclockwise tendency of the along- and cross-track errors vectors in the WPAC. Of interest is that this counterclockwise pattern of the along- and cross-track errors vectors coincides with, and is opposite to, the prevailing steering flows associated

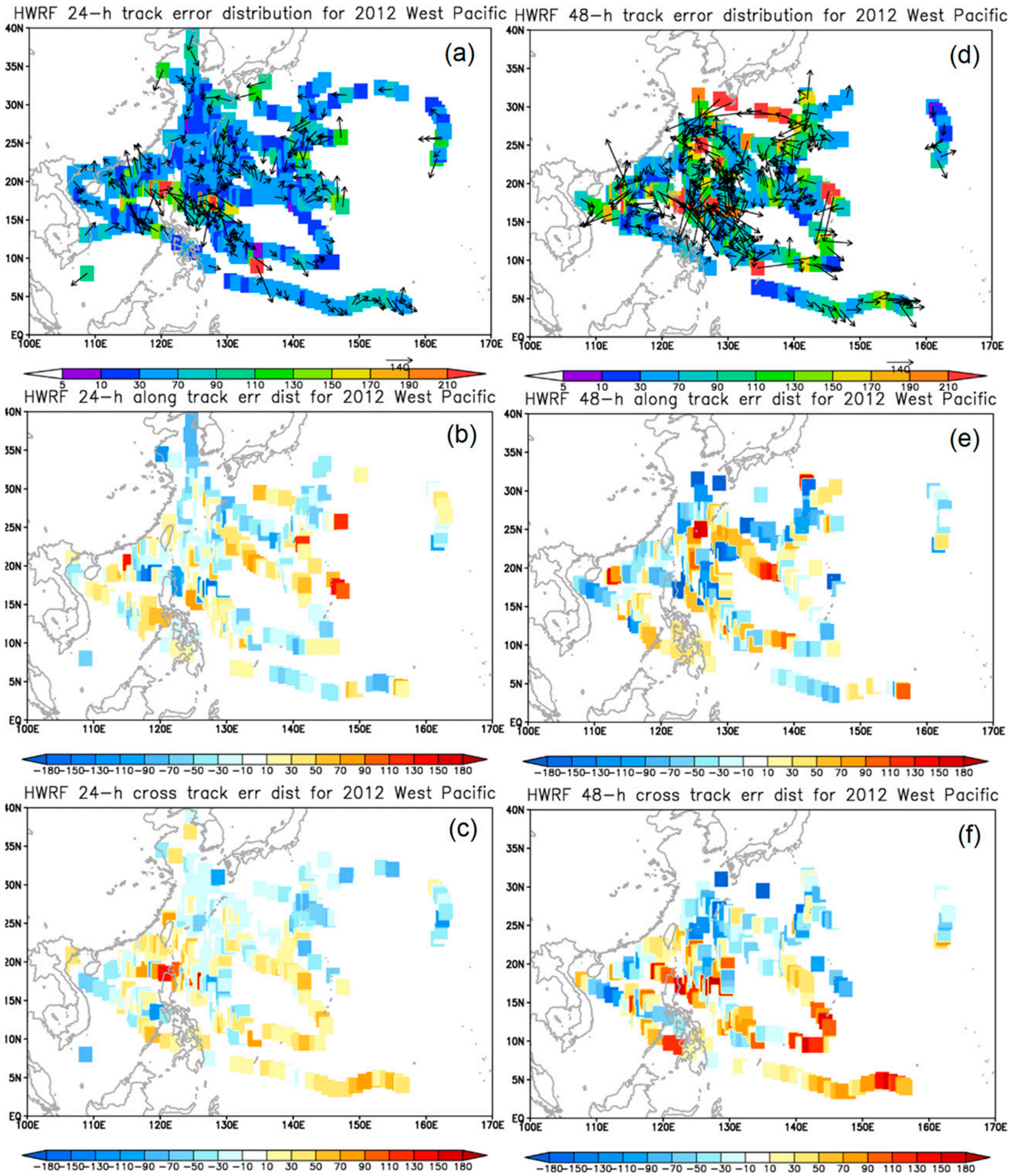

FIG. 2. (a) Distribution of the HWRF 24-h forecast absolute track errors (n mi; shaded) and the along- and cross-track errors (n mi; vectors) during 2012. (b) As in (a), but for only the 24-h along-track errors (n mi; shaded). (c) As in (a), but for only the 24-h cross-track errors (n mi; shaded). (d)–(f) As in (a)–(c), but for 48-h forecast errors. By convention, the arrows in (a),(d) pointing to the left (right) indicate the left (right) cross-track bias, and those pointing to the north (south) denote faster (slower) along-track biases.

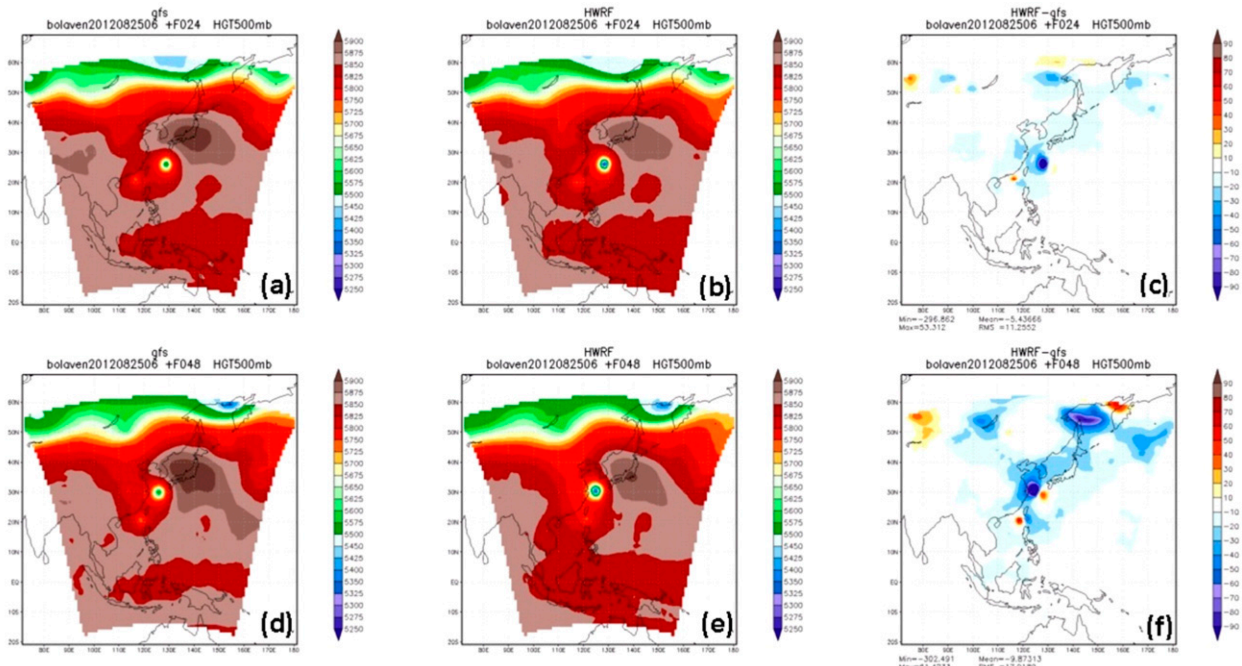

FIG. 3. (a) Horizontal cross section of the geopotential height (m; shaded) at 500 hPa from the GFS analysis valid at 0600 UTC 25 Aug 2012. (b) The HWRF 24-h forecast of the geopotential height (m; shaded) at 500 hPa valid at the same time as in (a). (c) The difference between HWRF and the GFS analysis. (d)–(f) As in (a)–(c), but for 48-h forecast lead time.

with the western Pacific subtropical high (WPSH). This resulting pattern of the along- and cross-track errors indicates that the track errors could have some connection to the development of the WPSH in HWRF. Specifically, HWRF tends to underestimate the strength of this large-scale feature, and so WPSH could not extend as far to the west, as seen from observation (cf. Fig. 6, described in greater detail below; TWAF). As a result, this weaker WPSH in the HWRF large-scale flow leads to a weaker steering flow, and so tends to shift the model storms too early to the north during their early life cycle near the southern edge of the WPSH. While the above connection of the cross-track errors with the weaker WPSH could not be fully revealed by simple statistics of the errors (see Fig. 5, described in greater detail below), the spatial correlation could at least help explain the dominantly positive cross-track bias in the bulk statistics of the cross-track errors seen in Fig. 1. Note that the cross-track errors are defined with respect to the direction of the storm motion and so it is not known in general if a positive (negative) error indicates a north (south) bias. However, because a majority of TCs in the WPAC move in the northwestward direction governed mostly by the WPSH, the right (left) biases in this analysis imply the biases to the north (south) in the low latitudes and south (north) in the higher latitudes. Thus, storms evolving along the southern edge of the WPSH tend to curve too much to the north, whereas those that developed on the northern side of the WPSH tend to have a left bias because of the weak WPSH system in the model.

Additional analyses of the HWRF outermost domain indeed indicate the weaker strength of the WPSH for a majority of cases during HWRF's real-time experiments in 2012, which was also seen during the 2013 real-time experiments (cf. Fig. 6, described in greater detail below; TWAF). As an example, the 24- and 48-h HWRF forecasts of the 500-hPa geopotential heights initialized at 0600 UTC 25 August 2012 are shown in Fig. 3. Along with the negative tendency along the coastline, one notices that the wide spread of the weaker development of the WPSH in this example cycle as compared to the GFS analysis could result in weaker steering currents. Such weaker large-scale steering flow is not limited to these particular instances, but in fact is seen in other cycles as well, causing a systematic right bias in the motion of the storms moving along the southern edge of the WPSH. This explains why storms at the edge of this subtropical high tend to move slower with a right bias (i.e., northeasterly bias), while those in the higher latitudes have a southwesterly bias.

Another noteworthy feature is that both along- and cross-track errors from HWRF tend to be larger in situations where there are multiple storms interacting

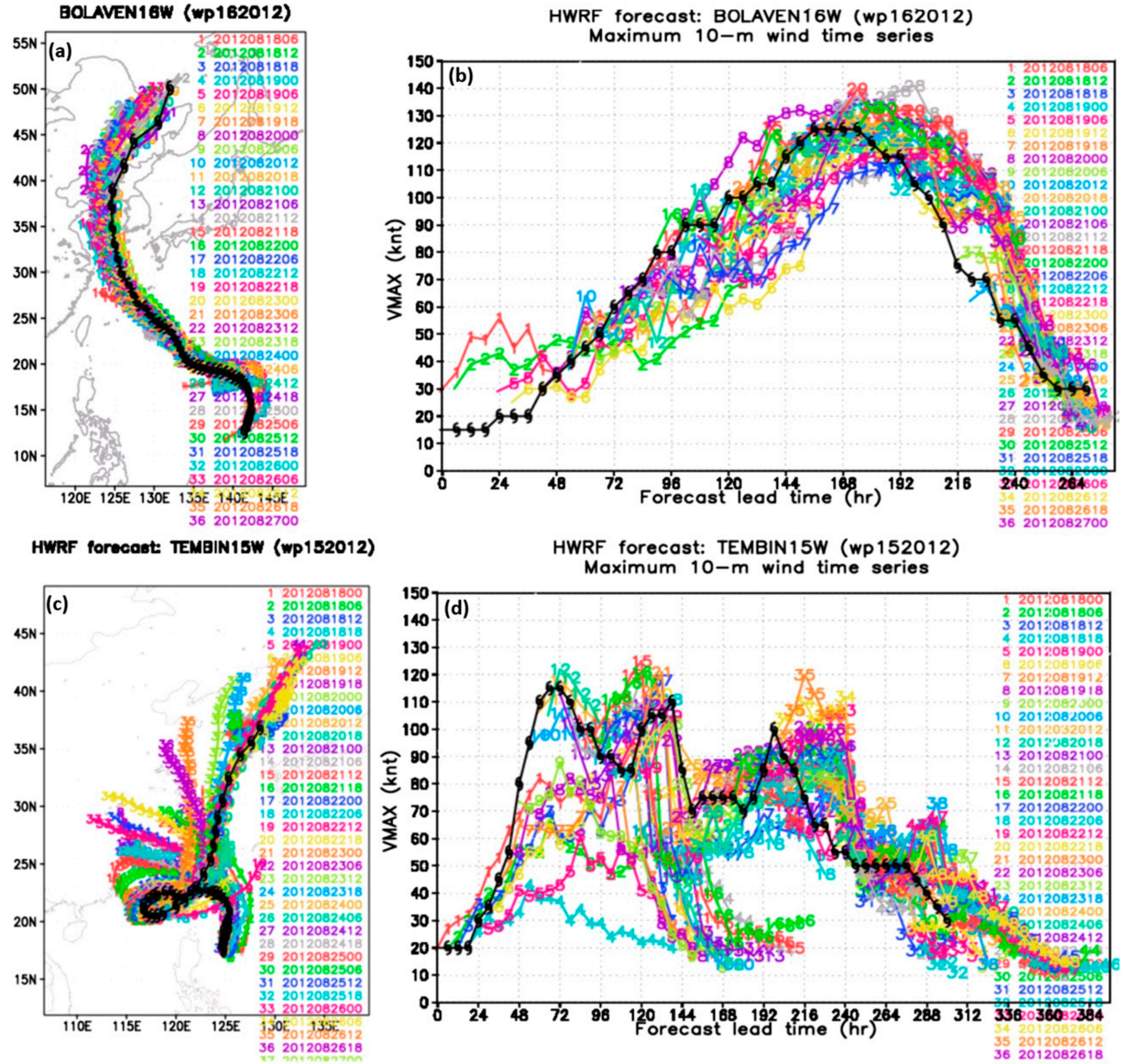

FIG. 4. Composite plots of the (a) track and (b) VMAX forecasts of Typhoon Bolaven (2012) from 0600 UTC 18 Aug to 0000 UTC 27 Aug 2012 with the smallest 5-day track forecast errors. (c),(d) As in (a),(b), but for Typhoon Tembin (2012) from 0000 UTC 18 Aug to 0000 UTC 29 Aug 2012 with the largest 5-day track forecast errors.

with each other, or when the storm is in close proximity to a landmass, consistent with previous studies in the WPAC (see, e.g., Kehoe et al. 2007; Payne et al. 2007). This observation appears to be realized in the real-time experiments with HWRF as well. An illustrative example is the pair of typhoons, Tembin (15W) and Bolaven (16W), that coexisted during August 2012. Figure 4 shows the composite plots of track forecasts during the entire life cycle of these two typhoons. While both track and intensity forecasts of Typhoon Bolaven (16W) show very good agreement with the best-track data, Typhoon Tembin (15W) seems to be much harder to predict because of its strong interaction with Typhoon Bolaven and with the complex topography over mainland China. Topographic influences of mainland China on observed and modeled typhoon tracks deserve more in-depth analysis, which will be carried out in a future study. Despite capturing the loop near the Hong Kong coast, there were a few cycles from 1200 UTC 19 August to 1200 UTC 21 August that showed HWRF forecasts for Typhoon Tembin seemed to be under another influence of the terrain and the large-scale trough nearby had caused Tembin to make landfall too early in those cycles. This kind of vortex–vortex interaction is consistent with previous studies, for example, by Brand (1970), Carr and Elsberry (1998), Prieto et al. (2003), Wu et al. (2003), and Kuo et al. (2008), which showed that a weaker vortex tends to orbit around a stronger, nearby vortex.

Depending on the intensity and size of the nearby vortex, the track of the weaker vortex could be heavily influenced by the development of the stronger one. The large cross-track errors associated with Typhoon Tembin in this specific example of the vortex binary interaction account for the dominant left bias near China's Hainan Island, which was not apparent from the mean statistics (cf. Fig. 1c). This example of Typhoon Tembin with large track forecast errors falls well into the high track error category reported by Payne et al. (2007), which shows that ~20% of the large track error cases are due to vortex–vortex interactions. This example of vortex–vortex interaction illustrates that a simple analysis of the averaged cross-track errors would not exhibit the full nature of the complex characteristics of the TC movement in this WPAC.

To examine the relationship between storm intensity and track errors for HWRF, Fig. 5 further stratifies the track forecast errors with respect to the storm initial intensity being stronger or weaker than the 50-knot (kt; $1\,\mathrm{kt} = 0.51\,\mathrm{m\,s^{-1}}$) threshold. This threshold usually represents storms that are better organized (initially strong) at or above 50-kt intensity, and less organized (initially weak) below 50-kt intensity. One can see that while there is somewhat better track forecast performance for strong storms (comparable to GFS track forecast errors at all times), it is apparent that the track forecast errors increase quite substantially when the storms are weak at the initial time. This is expected as the weak storms tend to be more sensitive to environmental influences (see, e.g., Nolan et al. 2007), especially when there is a nearby strong cyclonic system. The occurrence of the binary interactions should be emphasized as the WPAC has experienced increased TC activity in 2012 with five instances of more than two storms coexisting at the same time. We also observed that the cross-track errors have more significant differences between initially strong and initially weak storms (Figs. 5c and 5f), with most of the initially strong storms showing left-track biases (Fig. 5f) while initially weak storms exhibit right-track biases (Fig. 5c). This is consistent with the general northwestward movement of TCs, which implies that right-track bias tends to keep storms over the ocean while left-track bias brings storms closer to the continent, subjecting them to greater influence of topographic interactions (see, e.g., Chang 1982; Lin et al. 1999; Huang et al. 2011).

b. Intensity forecast verification

Figure 6 compares homogeneous real-time intensity forecast errors from the HWRF, GFDN, and COAMPS-TC for the 23 TCs in the WPAC during 2012 (from 03W to 25W) for which HWRF forecasts were available. It can be seen that although HWRF shows better performance for intensity at the early lead times, with its best performance during the first 24 h, the longer lead time intensity forecasts are significantly degraded, with the 5-day VMAX absolute errors reaching ~21 kt, with a small negative bias beyond 72 h into integration (Fig. 6b). This negative bias indicates that HWRF underestimates the storm intensity, especially at longer lead times. Note that HWRF uses a sophisticated vortex initialization system that matches the initial storm intensity to the observed estimates provided by JTWC in the form of tcvitals (Liu et al. 2012). As the model is integrated forward, the benefit of the better initialization appears to decrease quite significantly after 24–48 h of forecast, as the mean absolute intensity errors increase quickly from 5 to 14 kt within the first 24 h. Such faster error growth in intensity errors of HWRF is not limited to the WPAC, but is also observed in the EPAC and NATL (Tallapragada et al. 2012, 2014). The rapid increase of the absolute intensity errors during the first 48 h and the subsequent leveling off is generally seen in all regional models that have the vortex initialization component. This suggests that the benefit of the vortex initialization is most dominant during the first day or two, and it is the inherent model uncertainties in physics and representation of the large-scale environment that determine the intensity errors at longer forecast lead times.

Examination of the intensity forecast errors cycle by cycle shows that the landfalling cycles appear to have minimal impacts on the overall statistics of the intensity errors (Fig. 7). While the absolute intensity errors (Fig. 7b) do not show significant changes after all landfalling points in the best-track dataset are excluded in the verification, intensity biases (Fig. 7a) showed differences of the order of 20%, and tend to be somewhat smaller at most lead times. Further examination of the landfalling points shows that HWRF tends to produce stronger storms over land when the model storms are close to the coastlines, which generate less negative intensity bias that could offset the negative intensity bias for storms over ocean (not shown). As such, removing the landfalling points is found to actually decrease the negative intensity bias (Fig. 7a).

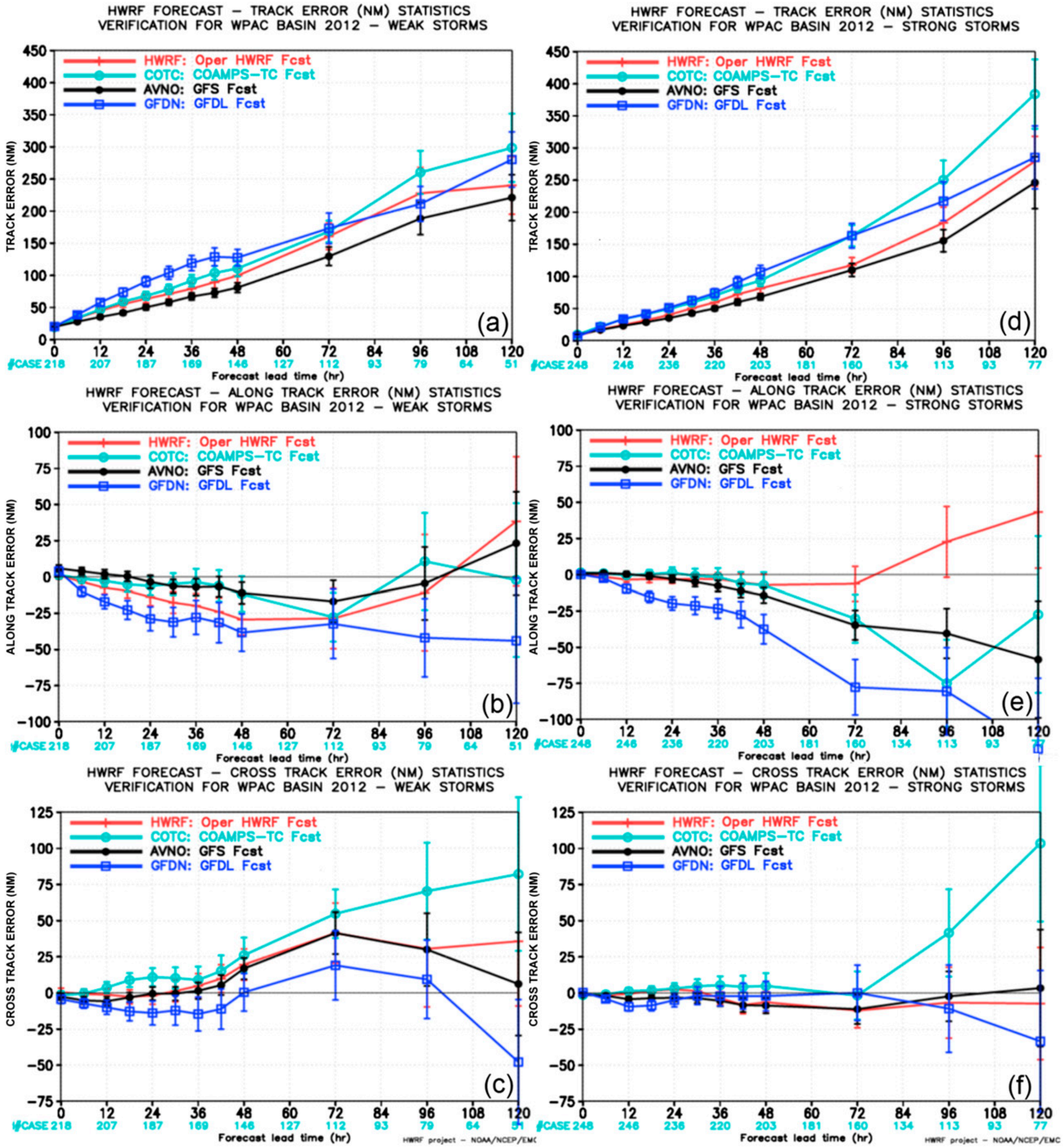

FIG. 5. As in Fig. 1, but for the verification of storms with initial VMAX (a)–(c) weaker and (d)–(f) stronger than 50 kt.

The irregular distribution of the storm intensity bias is more apparent from the geographical distribution of the intensity bias shown in Fig. 8. For example, prominent negative intensity bias is noted in the South China Sea and the ocean region to the southeast of Japan, whereas most of the overestimation of TC intensity is observed in the East China Sea region for both 24- and 48-h lead times. Physically, such a positive bias in intensity forecasts seems to have a connection to the slow bias of the track forecast in the East China Sea (Fig. 2) as the storms in this region tend to possess higher intensities. The HWRF-simulated storms to the southeast of Japan tend to have a slower translational speed as compared to the observed track with prolonged exposure to the warm ocean surface, resulting in higher intensity than observed, as noted in a previous study by Zeng et al. (2007).

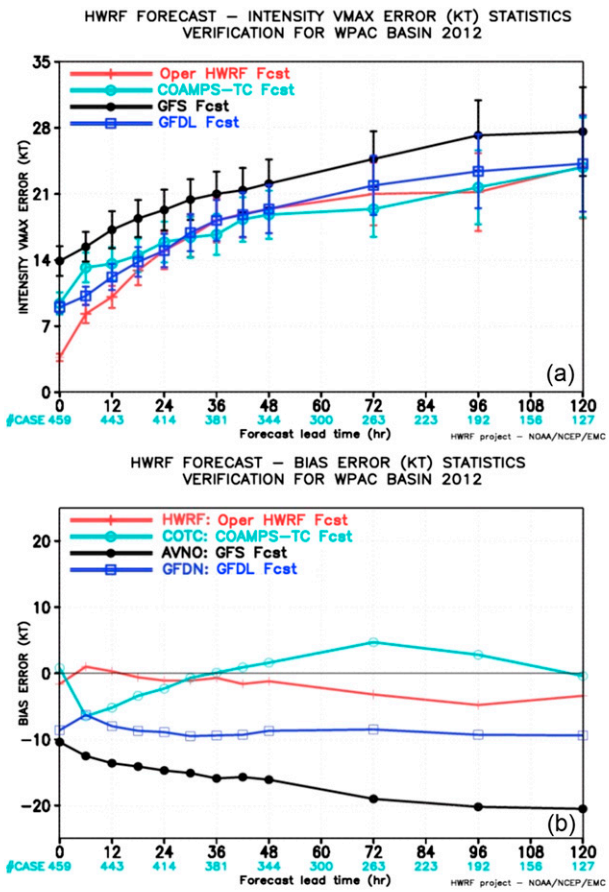

FIG. 6. As in Fig. 1, but for the mean intensity errors (kt) and the mean bias (kt).

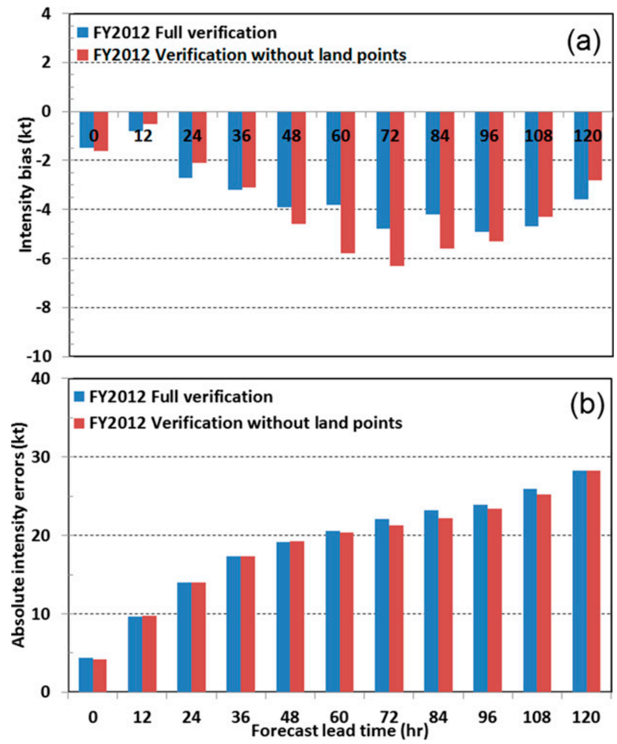

FIG. 7. Nonhomogenous comparison of the (a) HWRF intensity bias and (b) absolute intensity errors for the entire 2012 real-time experiment in the WPAC (blue columns) and for statistics with all landfalling points excluded (red columns).

The opposite is also reflected to some degree in the South China Sea region, to the east of Vietnam, where the simulated storms appear to move faster and make landfall earlier than observed, explaining for the negative intensity bias; that is, fast-moving storms have negative bias in contrast to slow-moving storms with positive intensity bias. Examples of Typhoons Tembin (15W) and Son-Tinh (24W) that are in close proximity to the Gulf of Tonkin are fairly illustrative for this negative intensity bias. The case of Typhoon Tembin is worth emphasizing as its interaction with Typhoon Bolaven has resulted in a complicated storm track, which greatly impacted the intensity forecasts because of incorrect landfall timing (cf. Fig. 4). For example, all cycles from 1800 UTC 19 August to 0000 UTC 23 August 2012 have incorrect landfall timings, which caused Tembin to weaken rapidly while the actual storm tracked out to the open ocean along the coastline and could manage to maintain its strength until making landfall in North Korea. Such a connection between the storm intensity bias and the track pattern is more apparent at the 48- than at the 24-h lead time (Fig. 8), indicating that the storm translational speed has a direct influence on the storm intensity at longer lead times.

Stratification of the intensity absolute errors and bias based on the storm initial intensity (similar to that for track verification analysis shown in Fig. 3) is shown in Fig. 9. HWRF has issues with the weaker systems for which it substantially underestimates the storm intensity at all forecast lead times, while the model overestimates the storm intensity for strong storms (Fig. 9d). In addition, weak storms tend to have larger absolute intensity errors as compared to the strong storms at the longer forecast lead times; the 4- and 5-day absolute intensity errors for weak storms are ~26 and 25 kt, respectively, whereas the corresponding intensity errors for strong storms are ~20 and 22 kt. Such underestimation of the storm intensity from HWRF for the weaker storms with larger-amplitude errors is of concern, and could be related to the quicker dissipation (or faster landfall) of a few TCs. Dissipation of weaker storms has a direct impact on the capability of the HWRF nests to follow the vortex center, which could amplify the absolute intensity errors when the nest loses the storm as a result of dissipation.

TCs in the WPAC tend to exhibit rapid changes in intensity where conditions for rapid intensification (RI) occur more frequently (see, e.g., Brand 1973; Ventham

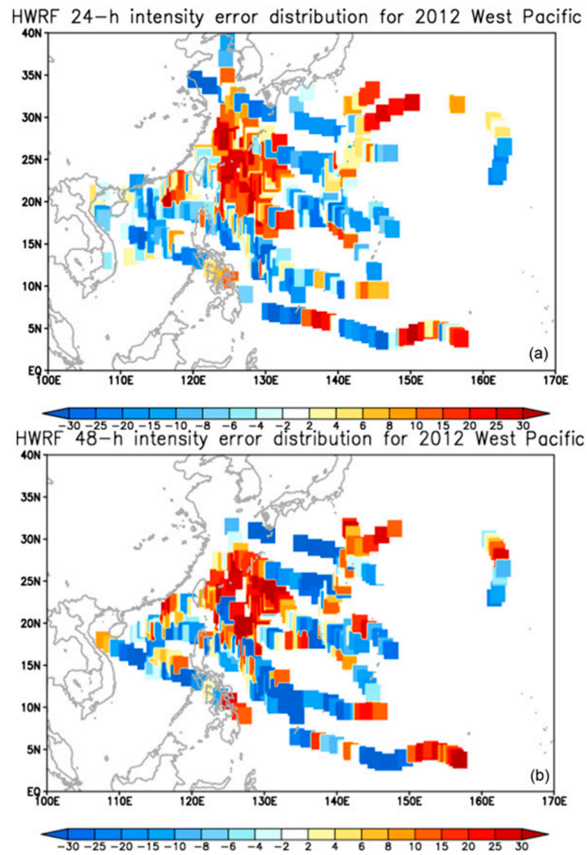

FIG. 8. Distribution of the HWRF intensity bias (kt; shaded) in the WPAC during 2012 for the (a) 24- and (b) 48-h forecast lead times.

and Wang 2007). The capability of HWRF in capturing RI of TCs is examined in Fig. 10, which shows a scatterplot of the 24-h changes of VMAX obtained from HWRF along with the best-track dataset. Here, the RI criterion is defined as an intensity change of +30 kt $(24\,\mathrm{h})^{-1}$, and HWRF is found to underestimate RI quite significantly. Of 306 RI occurrences, HWRF could capture only 45 of those instances and produced 261 misses. This would correspond to a probability of detection (POD) index of ~0.15, which is fairly low. However, if one defines an intensification event simply when the 24-h change of VMAX is larger than zero for both the model forecasts and the observed intensity, the POD index is significantly higher (~0.4). This suggests that HWRF dynamics has some internal constraints that prevent it from intensifying the storms rapidly as compared to observations. Such underestimation of RI with HWRF is noted for other basins as well. It should be mentioned here that the analysis of RI is currently of special interest to forecasters and modelers, as this could demonstrate the capability of the high-resolution tropical cyclone models operating at convective-resolving scales. While the bulk error statistics could provide some preliminary evaluation of the model performance, it is the RI verification and stratification of intensity verification that could help demonstrate the benefits of the high-resolution models and help identify areas where further development is needed.

c. *Radii forecast verification*

One of the most significant improvements to 2012's HWRF version over previous operational versions is the ability to capture better storm structure (Tallapragada et al. 2012, 2014). While most of the TC forecast verifications have relied so far on the few basic metrics of the track, intensity, and bias errors, recent studies have shown the necessity of verifying the horizontal structure of the storms, considering that such structure information has direct impacts on various downstream applications such as wave models, storm surge warning, or rainfall, flooding, and inundation forecasts. In this regard, it is of interest to evaluate the performance of HWRF's surface wind structure as compared to other dynamical models, quantified in terms of the wind radii at four different quadrants analyzed and reported by JTWC. Here, the wind radii at each quadrant are defined as the maximum distance from the vortex center that could match each wind threshold.

Figure 11 shows the mean 34- (R34), 50- (R50), and 64-kt (R64) radii verifications, which are obtained by taking an average of the radii over four different quadrants for the entire season. As a result of the limited information available from the GFDN datasets, we only compared the radii information obtained from COAMPS-TC, HWRF, and GFS. Overall, HWRF performs quite well for both R34 and R50, with storm size errors that are smaller as compared to COAMPS-TC and comparable to the GFS forecasts. In particular, the radii verification shows significant improvement not only at the initial time but for the entire forecast period. Although the initial R34 error is ~25 n mi, it manages to get smaller and stabilizes at around 5 n mi at all lead times. This indicates that the improved representation of the horizontal wind structure for NATL and EPAC noted in the 2012 operational HWRF configuration (Tallapragada et al. 2014) is also realized in the WPAC. The R50 verification shows however that HWRF storm structure for stronger storms tends to excessively contract toward the end of the 5-day forecast (assuming the actual storms are contracting during their intensification), while the R64 bias is still mostly positive. Similar large R50 values are also noticed in the NATL and EPAC regions, and seem to be related to the substantial convergence within the inner-core region (Tallapragada et al. 2014). Sensitivity experiments

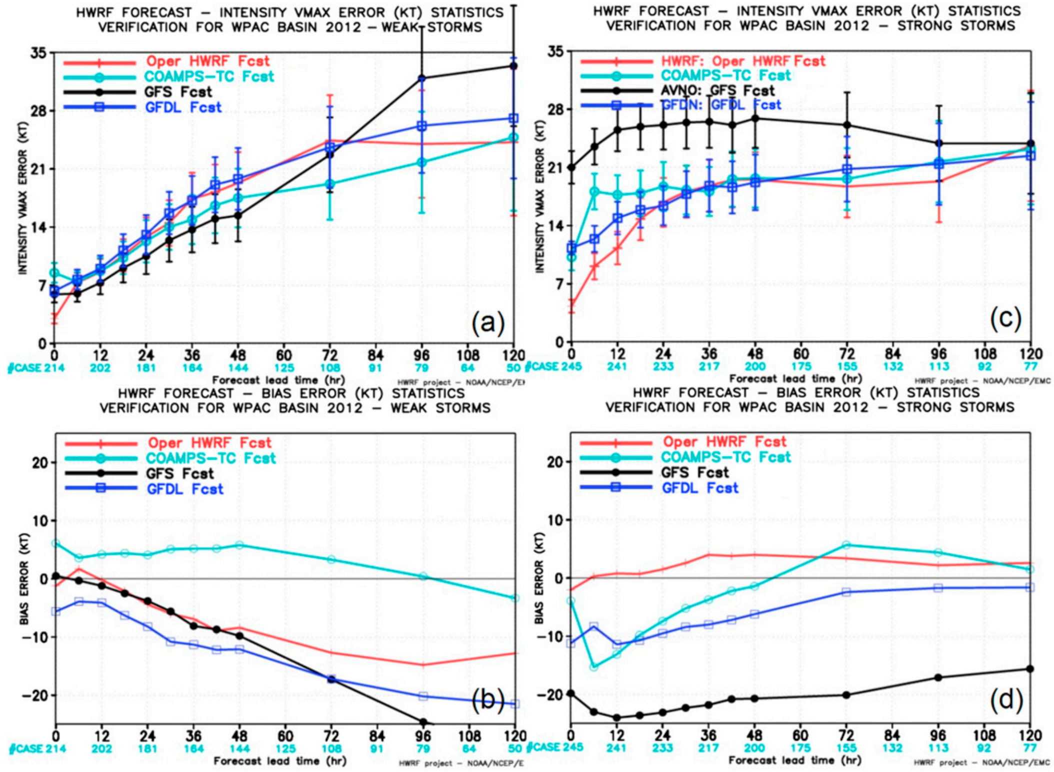

FIG. 9. As in Fig. 5, but only for the intensity and bias verification of (a),(b) weak and (c),(d) strong storms.

conducted at NCEP/EMC showed that the larger model storm radii as compared to the observed radii can be reduced by the use of a more representative mesoscale (scale aware) cumulus convection scheme (not shown).

Unlike the EPAC or NATL, we observe however that the inner-core R64 of HWRF shows a much different structure in the WPAC with an overall broader R64 size. While COAMPS-TC shows a persistent broadening of the storm size across all wind radii with forecast lead times, HWRF tends to possess stable R64 errors with time. It should be noted that statistics for the R64 in general contain larger uncertainty because of a lack of observations within the inner-core region, especially for stronger TCs. In addition, different model resolutions make it hard to have a meaningful comparison of the R64 information. However, the general overestimation of HWRF's R64, which represents the inner-core structure of the model storms, could still indicate that the physics schemes used in HWRF may not be sufficient to properly resolve the storm's inner-core structure. This structure verification is a high priority area of research supported by NOAA's HFIP (Gall et al. 2013) that we would like to present in our future study.

Although there may be some particular cycles in which information from different quadrants may not be consistent and may affect the overall structural verification for these cases, the statistics for ~500 cycles are sufficiently robust to represent the general radii statistics of the model. While such radii statistics cannot directly depict the TC structure or be applied to a specific storm, the consistency among the model storm's outer size (i.e., 34-kt radii), and its inner size (i.e., 50- and 64-kt radii), VMAX, PMIN, and RMW, is a necessary criterion for any model because all of these variables indicate how well the model dynamical constraints are maintained in real-time TC forecasts. Of course, verification of the 3D structure of TCs would require much more than the simple radii statistics, but from the operational perspective, the radii so far is the only additional information that is available for model evaluation. Thus, any improvement in the model storm size is a good indicator that the model dynamics and TC structure have been effectively represented.

d. Verification of dynamical constraints

Vortex initialization is one of the important components of the operational TC forecasting models. This is needed because the initial vortex generated directly from the global model is often much weaker and broader than the observations, especially when storms attain

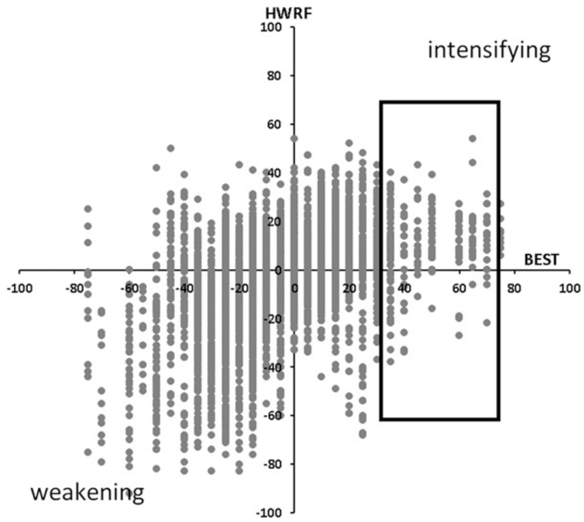

FIG. 10. Scatterplot of 24-h VMAX change (kt; dots) obtained from HWRF (ordinate) and best track (abscissa) during the 2012 real-time experiment in the WPAC. The upper-right quadrant corresponds to an intensifying phase, while the lower-left quadrant indicates the weakening of the WPAC typhoons. The black box denotes the points for which an observation indicates a 24-h VMAX change is >30 kt, which is used for computing the RI detection.

higher intensities (cf. Fig. 6) for which the initial difference between the GFS vortex and the observations could be as large as 50 kt in some cases. The vortex initialization procedure employed by HWRF is designed to accurately represent the initial intensity as reported by NHC/JTWC (Liu et al. 2012; Gopalakrishnan et al. 2012a). Evaluation of the performance of the vortex initialization component can be done by monitoring the vortex spinup–spindown during the first several hours of model integration. Since the environmental conditions are different among different ocean basins, the characteristics of the model's initial intensity changes may vary as well. In this regard, the correlation of changes in VMAX and PMIN during the first 6 h of model integration, a typical measure for the model initial vortex adjustment, can provide some useful information as to how effective the vortex initialization is in the HWRF system. An ideal vortex initialization scheme would require a consistent change of VMAX and PMIN during the initial adjustment, and a minimum time for the balanced adjustment such that the model vortex can develop internal dynamics consistent with the model environment as quickly as possible. Physically, the former requirement implies that the increase of VMAX will correspond to the deepening of PMIN (and vice versa), whereas the latter requirement is important as it allows the model vortex to adapt to its environment consistently within the model in a reasonable time frame (usually in the first few hours of integration).

Figure 12 shows the distribution of the 6-h changes of VMAX and PMIN for different intensity bins. While the magnitude of the 6-h changes of VMAX and PMIN is relatively small as expected, there are two issues one can notice with HWRF vortex initialization. First, there is a range of intensity bins from 30 to 65 kt (depression to category-1 stage) in which HWRF shows an unexpected positive correlation of the 6-h changes of VMAX and PMIN. For example, the 6-h change of VMAX for the 35–40-kt bin is ~5 kt, indicating that the model storms intensify in general, whereas the corresponding PMIN change is ~1–2 hPa, which implies that the model storms weaken. This unexpected behavior could be related to storm size adjustments in the model that is not fully understood at this moment, but the sensitivity experiments conducted during the implementation of HWRF at EMC seem to indicate that this is due to the procedures used in vortex initialization, which constrains only VMAX, R34, and RMW with no explicit adjustment of the PMIN information during the initialization steps. As discussed in Tallapragada et al. (2012, 2014) and Liu et al. (2012), the main reason for PMIN not being constrained is because the gradient wind balance that allows for obtaining PMIN from VMAX and RMW tends to underestimate the actual PMIN, especially within the PBL where the nongradient wind balance dominates. As a result, the constraint on PMIN is not well preserved by the gradient wind balance, and PMIN is therefore left to be adjusted by the model dynamics rather than being forced to match with observed values. This could explain some of the unexpected behaviors of the 6-h changes observed in Fig. 12.

The second issue that can be seen in Fig. 12 is the large magnitude of the 6-h intensity changes at strong wind speeds. Physically, the negative change of VMAX is often expected at the high-intensity regime because storms often reach their peak strength (i.e., the maximum potential intensity) at this limit and thus normally weaken as they make landfall or move into higher latitudes. While the VMAX changes for the 100–110-kt bin show a negative drop of VMAX that partly reflects this fact, the magnitude of the changes appears to be fairly large, indicating that HWRF tends to spin down too fast. Another peculiar aspect is that at the higher-intensity bins (>130 kt), the 6-h changes do not show similar spindown as it is supposed to be; for example, the 6-h VMAX change is only about −1 kt for the 110–130-kt bin, and nearly zero for the 130-kt bin, whereas the PMIN changes are much more negative (i.e., the model storms keep deepening). The irregular VMAX and PMIN changes at the higher wind regime indicate that the vortex initialization procedure for storms stronger than category-3 needs to be carefully evaluated for its

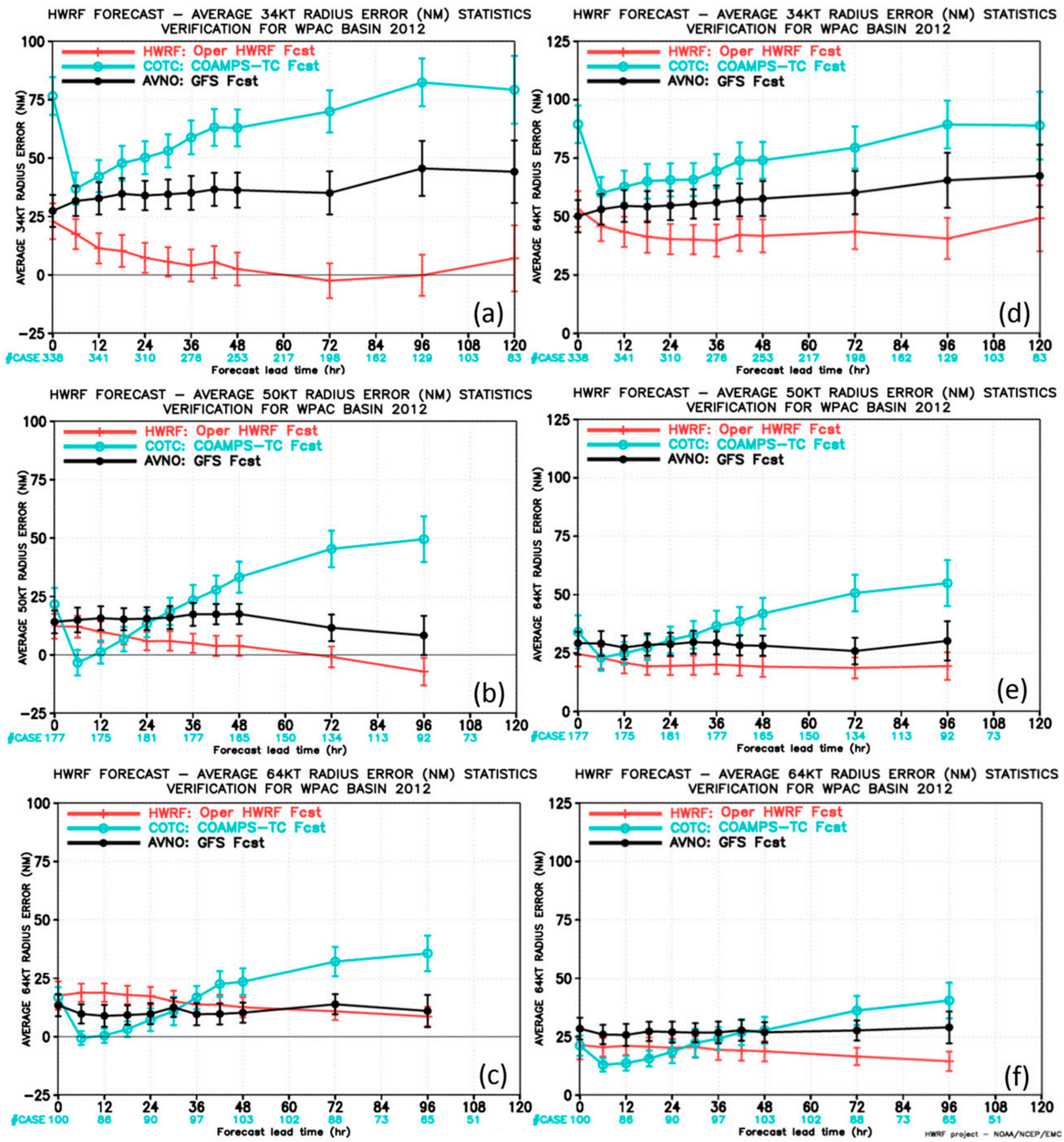

FIG. 11. Homogenous verification of mean (a) 34-, (b) 50-, and (c) 64-kt wind radii bias errors of HWRF (red), COAMPS-TC (blue), and AVNO (black) during the 2012 real-time experiment. (d)–(f) As in (a)–(c), but for the absolute wind radii errors.

effectiveness. The vortex adjustment processes in the initialization procedure are probably leading to the model initial vortex structure not being consistent with the environment the vortex is embedded into, along with inadequate resolution and physics to support such strong intensities at the initial time. The stochastic nature of this spin up and spin down comes from uncertainty in the storm size estimates as well as the vertical structure representation (Vukicevic et al. 2013). Note that in HWRF we do not initialize clouds in the initial state, and the thermodynamic response comes from model equations during the integration.

To further examine the dynamical constraints imposed by the pressure–wind relationship, Fig. 13 shows a

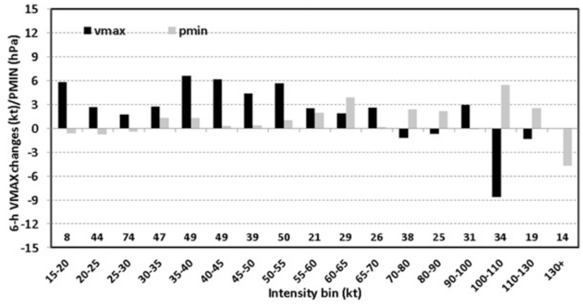

FIG. 12. Stratification of the change in the VMAX (kt; black columns) and PMIN (hPa; gray columns) during the first 6 h of model integration for the WPAC real-time experiments obtained from HWRF.

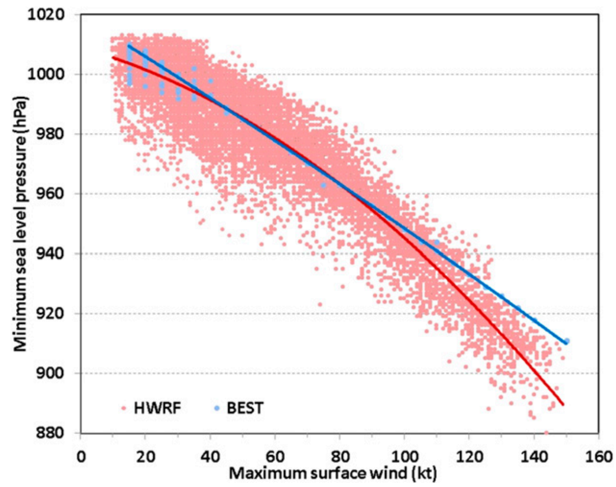

FIG. 13. Scatterplot of the VMAX and PMIN from the 2012 real-time experiments in the WPAC with HWRF. Blue dots denote the observational forecast values, and red dots denote the model forecast values. Solid lines are the second-order polynomial best fit.

scatterplot of VMAX and PMIN obtained from HWRF in the WPAC during the entire experimental period in 2012 and from the best-track data along with the best-fit second-order polynomial curves. It should be mentioned that although the best-fit curve for the best-track data (blue solid curve) looks to be nearly perfectly fit, this does not mean that the observed PMIN and VMAX are matched to such a degree. In fact, the so-called observed PMIN data from the best-track dataset are often not observed directly but, rather, are derived from a given pressure–wind relationship based on the Dvorak technique (Velden et al. 2006). Unlike the best-track data for PMIN and VMAX in the NATL that are usually obtained independently and probably more accurately, the PMIN values in the WPAC are rarely directly observed but mostly inferred from satellite images and a prescribed pressure–wind relationship. This provides an explanation for the near-perfect best-fit curve for the best-track data, as seen in Fig. 13. While comparison of the model VMAX and PMIN values against such a best-fit curve could not fully capture the characteristics of the pressure–wind relationship, it could at least give us some information about the dynamical constraints of HWRF with respect to the prescribed statistics (assuming that the prescribed pressure–wind relationship could be trained and valid for the WPAC). HWRF appears to provide consistent values of VMAX and PMIN for a range of intensities up 80 kt; afterward, this relationship starts to deflect from the best-track distribution (see the red solid curve in Fig. 13). Specifically, the HWRF PMIN appears to be lower than the best-track values during a strong wind regime, given the same VMAX. This could be attributed again partly to the fact that PMIN is not constrained during the vortex initialization as discussed earlier, thus generating a mismatch between modeled and observed PMIN at the initial time. On the other hand, such a difference between the model values and the best-track values could also be due to the prescribed pressure–wind relationship that is used to generate PMIN for the best track, which may not fully reflect the connection between VMAX and PMIN for the high-intensity limits. Of significance is that even though the same model configuration has been implemented, HWRF showed a much more consistent pressure–wind relationship with the observations in the NATL or EPAC (Tallapragada et al. 2014). The departure from the pressure–wind relationship at higher wind speeds for the WPAC may therefore indicate that the TCs in the WPAC could possess some distinct characteristics that the model is not fully capable of forecasting. Lack of ocean coupling for HWRF in the WPAC contributes further to this issue, as it does not allow for cooling due to upwelling. This could also help explain the overestimation of the TC intensity for strong storms, as seen in Fig. 9d.

4. Summary and conclusions

In this work, we have summarized recent efforts of the hurricane modeling team at NCEP/EMC in implementing the operational HWRF for real-time TC forecasts for the first time in the WPAC during the period from July to December 2012. Evaluation of the model performance showed that HWRF outperformed other regional models in track forecast errors with the 3-, 4-, and 5-day track errors being ~125, 220, and 290 n mi, respectively. Intensity forecasts also showed better performance seen during the first 24 h; the 3-, 4-, and 5-day maximum 10-m wind errors are 19, 19, and 22 kt, respectively. Further stratification of the track and absolute intensity forecast errors with respect to the storm initial intensity revealed that HWRF tends to underestimate the storm intensity for weak storms, but overestimate the storm intensity for strong storms.

Additional analyses of the distribution of the track and intensity errors over the WPAC suggested that HWRF possesses a systematic negative intensity bias, slower movement, and a right bias in the lower latitudes. However, in the higher latitudes to the east of the East China Sea, HWRF has a positive intensity bias as well as faster storm movement. The broad pattern of along- and cross-track errors is dominated by the counterclockwise direction that opposes the large-scale anticyclonic steering flow associated with the subtropical high in the WPAC. This suggests that HWRF underestimated the development of the large-scale pattern of the subtropical high, leading to weaker steering flow that resulted in such a counterclockwise distribution of the along- and cross-track errors.

Verification of the 34-, 50-, and 64-kt radii showed that HWRF generally has better storm size and horizontal structure forecasts as compared to other models. Except for the fairly larger 50-kt radii toward the end of the 5-day forecast, the averaged bias errors of storm radii at all four different quadrants are reasonable not only at the initial time, but also for the entire forecast period. Such stable storm size error statistics are not only seen in the bias errors but also applied to the absolute radii errors, which indicates that the storm-scale dynamics with respect to horizontal wind structure is well reflected within HWRF. In addition to these storm size verifications, the dynamical constraints between the minimum sea level pressure and the maximum wind, as well as the initial changes of these metrics during the first 6 h of integration, also demonstrated that the FY 2012 version of HWRF could at least capture the storm dynamics as well as account for the adjustment of the vortex initial balance.

Although both track and intensity forecast errors of HWRF in the WPAC are somewhat larger than those in the NATL or EPAC, which could be due to the lack of inner-core data assimilation and ocean coupling, performance during 2012 shows that HWRF has some promising capability as compared to a suite of regional models used by JTWC. Real-time experimental forecasts from HWRF were made available to JTWC with more than 85% on-time delivery capability. The real-time experiments were continued in 2013 at the request of JTWC and with continued support from HIFP, and TWAF will document our evaluation of HWRF's real-time forecast performance for the 2013 WPAC TCs with specific focus on the model's vortex structure, genesis predictability, and capability of forecasting rapid intensification, apart from addressing some important model deficiencies noted in the evaluation of forecast errors for the 2012 WPAC TCs using the upgraded 2013 version of HWRF.

Acknowledgments. This work was supported by the Hurricane Forecasting Improvement Project (HFIP) of NOAA. The EMC HWRF team would like to acknowledge various sources of constructive feedback and suggestions from the JTWC during the 2012 real-time WPAC experiments, which helped improve the 2012 HWRF forecast capability. We thank Lauren Carter for her assistance in carefully proofreading this manuscript.

REFERENCES

Arakawa, A., and V. R. Lamb, 1977: Computational design of the basic dynamical processes of the UCLA general circulation model. *Methods in Computational Physics*, J. Chang, Ed., Vol. 17, Academic Press, 173–265.

Bender, M. A., I. Ginis, R. Tuleya, B. Thomas, and T. Marchok, 2007: The operational GFDL hurricane–ocean prediction system and a summary of its performance. *Mon. Wea. Rev.*, **135**, 3965–3989, doi:10.1175/2007MWR2032.1.

Brand, S., 1970: Interaction of binary tropical cyclones of the western North Pacific Ocean. *J. Appl. Meteor.*, **9**, 433–441, doi:10.1175/1520-0450(1970)009<0433:IOBTCO>2.0.CO;2.

——, 1973: Rapid intensification and low-latitude weakening of tropical cyclones of the western North Pacific Ocean. *J. Appl. Meteor.*, **12**, 94–103, doi:10.1175/1520-0450(1973)012<0094:RIALLW>2.0.CO;2.

Brown, D. P., J. L. Beven, J. L. Franklin, and E. S. Blake, 2010: Atlantic hurricane season of 2008. *Mon. Wea. Rev.*, **138**, 1975–2001, doi:10.1175/2009MWR3174.1.

Cangialosi, J. P., and J. L. Franklin, 2013: 2012 National Hurricane Center verification report. NOAA/National Hurricane Center, 79 pp. [Available online at http://www.nhc.noaa.gov/verification/pdfs/Verification_2012.pdf.]

Carr, L. E., and R. L. Elsberry, 1998: Objective diagnosis of binary tropical cyclone interactions for the western North Pacific basin. *Mon. Wea. Rev.*, **126**, 1734–1740, doi:10.1175/1520-0493(1998)126<1734:ODOBTC>2.0.CO;2.

——, and ——, 2000: Dynamical tropical cyclone track forecast errors. Part I: Tropical region error sources. *Wea. Forecasting*, **15**, 641–661, doi:10.1175/1520-0434(2000)015<0641:DTCTFE>2.0.CO;2.

Chang, S. W.-J., 1982: The orographic effects induced by an island mountain range on propagating tropical cyclones. *Mon. Wea. Rev.*, **110**, 1255–1270, doi:10.1175/1520-0493(1982)110<1255:TOEIBA>2.0.CO;2.

Dickerman, C. L., 2006: A recent history of the GFDN Tropical Cyclone Forecast Model. Preprints, *27th Conf. on Hurricanes and Tropical Meteorology*, Monterey, CA, Amer. Meteor. Soc., P5.8. [Available online at https://ams.confex.com/ams/pdfpapers/108054.pdf.]

Doyle, J. D., and Coauthors, 2011: Real time tropical cyclone prediction using COAMPS-TC. *Atmospheric Science and Ocean Sciences*, C.-C. Wu and J. Gan, Eds., Advances in Geosciences, Vol. 28, World Scientific, 15–28.

Evans, A. D., and R. J. Falvey, 2013: Annual Joint Typhoon Warning Center tropical cyclone report. Joint Typhoon

Warning Center, 118 pp. [Available online at http://www.usno.navy.mil/NOOC/nmfc-ph/RSS/jtwc/atcr/2012atcr.pdf.]

Ferrier, B. S., 1994: A double-moment multiple-phase four-class bulk ice scheme. Part I: Description. *J. Atmos. Sci.*, **51**, 249–280, doi:10.1175/1520-0469(1994)051<0249:ADMMPF>2.0.CO;2.

Gall, R., J. Franklin, F. Marks, E. N. Rappaport, and F. Toepfer, 2013: The Hurricane Forecast Improvement Project. *Bull. Amer. Meteor. Soc.*, **94**, 329–343, doi:10.1175/BAMS-D-12-00071.1.

Gopalakrishnan, S., and Coauthors, 2012a: Hurricane Weather Research and Forecasting (HWRF) model: 2012 scientific documentation. NCAR Development Testbed Center Rep., 96 pp. [Available online at http://www.dtcenter.org/HurrWRF/users/docs/index.php.]

——, S. Goldenberg, T. Quirino, X. Zhang, F. Marks, K.-S. Yeh, R. Atlas, and V. Tallapragada, 2012b: Toward improving high-resolution numerical hurricane forecasting: Influence of model horizontal grid resolution, initialization, and physics. *Wea. Forecasting*, **27**, 647–666, doi:10.1175/WAF-D-11-00055.1.

Han, J., and H.-L. Pan, 2011: Revision of convection and vertical diffusion schemes in the NCEP Global Forecast System. *Wea. Forecasting*, **26**, 520–533, doi:10.1175/WAF-D-10-05038.1.

Hogan, T. F., and T. E. Rosmond, 1991: The description of the Navy Operational Global Atmospheric System's spectral forecast model. *Mon. Wea. Rev.*, **119**, 1786–1815, doi:10.1175/1520-0493(1991)119<1786:TDOTNO>2.0.CO;2.

Huang, Y. H., C.-C. Wu, and Y. Wang, 2011: The influence of island topography on typhoon track deflection. *Mon. Wea. Rev.*, **139**, 1708–1727, doi:10.1175/2011MWR3560.1.

Janjic, Z., 2003: A nonhydrostatic model based on a new approach. *Meteor. Atmos. Phys.*, **82**, 271–285, doi:10.1007/s00703-001-0587-6.

——, J. P. Gerrity Jr., and S. Nickovic, 2001: An alternative approach to nonhydrostatic modeling. *Mon. Wea. Rev.*, **129**, 1164–1178, doi:10.1175/1520-0493(2001)129<1164:AAATNM>2.0.CO;2.

——, R. Gall, and M. E. Pyle, 2010: Scientific documentation for the NMM solver. NCAR Tech. Note NCAR/TN-477+STR, 54 pp. [Available online at http://nldr.library.ucar.edu/repository/assets/technotes/TECH-NOTE-000-000-000-845.pdf.]

Kehoe, R. M., M. A. Boothe, and E. L. Elsberry, 2007: Dynamical tropical cyclone 96- and 120-h track forecast errors in the western North Pacific. *Wea. Forecasting*, **22**, 520–538, doi:10.1175/WAF1002.1.

Kleist, D. T., K. Ide, J. Whitaker, J. C. Derber, D. Parrish, and X. Wang, 2011: Expanding the GSI-based hybrid ensemble-variational system to include more flexible parameter settings. *Proc. 15th Symp. on Integrated Observing and Assimilation Systems for the Atmosphere, Oceans and Land Surface*, Seattle, WA, Amer. Meteor. Soc., J16.4. [Available online at https://ams.confex.com/ams/91Annual/webprogram/Paper180096.html.]

Kuo, H.-C., W. H. Schubert, C.-L. Tsai, and Y.-F. Kuo, 2008: Vortex interactions and barotropic aspects of concentric eyewall formation. *Mon. Wea. Rev.*, **136**, 5183–5198, doi:10.1175/2008MWR2378.1.

Kurihara, Y., R. E. Tuleya, and M. A. Bender, 1998: The GFDL Hurricane Prediction System and its performance in the 1995 hurricane season. *Mon. Wea. Rev.*, **126**, 1306–1322, doi:10.1175/1520-0493(1998)126<1306:TGHPSA>2.0.CO;2.

Kwon, Y., S. Lord, B. Lapenta, V. Tallapragada, Q. Liu, and Z. Zhang, 2009: Sensitivity of air–sea exchange coefficients (Cd and Ch) on hurricane intensity. Preprints, *29th Conf. on Hurricanes and Tropical Meteorology*, Tucson, AZ, Amer. Meteor. Soc., 13C.1. [Available online at https://ams.confex.com/ams/pdfpapers/88063.pdf.]

Landsea, C. W., and J. L. Franklin, 2013: Atlantic hurricane database uncertainty and presentation of a new database format. *Mon. Wea. Rev.*, **141**, 3576–3592, doi:10.1175/MWR-D-12-00254.1.

Lin, Y.-L., J. Han, D. W. Hamilton, and C.-Y. Huang, 1999: Orographic influence on a drifting cyclone. *J. Atmos. Sci.*, **56**, 534–562, doi:10.1175/1520-0469(1999)056<0534:OIOADC>2.0.CO;2.

Liu, Q., X. Zhang, S. Trahan, and V. Tallapragada, 2012: Extending operational HWRF initialization to triple-nest HWRF system. *Proc. 30th Conf. on Hurricanes and Tropical Meteorology*, Ponte Verde, FL, Amer. Meteor. Soc., 14A.6. [Available online at https://ams.confex.com/ams/30Hurricane/webprogram/Paper204853.html.]

Nolan, D. S., E. D. Rappin, and K. A. Emanuel, 2007: Tropical cyclogenesis sensitivity to environmental parameters in radiative–convective equilibrium. *Quart. J. Roy. Meteor. Soc.*, **133**, 2085–2107, doi:10.1002/qj.170.

——, J. A. Zhang, and D. P. Stern, 2009: Evaluation of planetary boundary layer parameterizations in tropical cyclones by comparison of in situ observations and high-resolution simulations of Hurricane Isabel (2003). Part I: Initialization, maximum winds, and the outer-core boundary layer. *Mon. Wea. Rev.*, **137**, 3651–3674, doi:10.1175/2009MWR2785.1.

Payne, K. A., R. L. Elsberry, and M. A. Boothe, 2007: Assessment of western North Pacific 96- and 120-h track guidance and present forecastability. *Wea. Forecasting*, **22**, 1003–1015, doi:10.1175/WAF1030.1.

Pike, A. C., and C. J. Neumann, 1987: The variation of track forecast difficulty among tropical cyclone basins. *Wea. Forecasting*, **2**, 237–241, doi:10.1175/1520-0434(1987)002<0237:TVOTFD>2.0.CO;2.

Prieto, R., B. D. McNoldy, S. R. Fulton, and W. H. Schubert, 2003: A classification of binary tropical cyclone–like vortex interactions. *Mon. Wea. Rev.*, **131**, 2656–2666, doi:10.1175/1520-0493(2003)131<2656:ACOBTC>2.0.CO;2.

Sampson, C. R., and A. J. Schrader, 2000: The Automated Tropical Cyclone Forecasting system (version 3.2). *Bull. Amer. Meteor. Soc.*, **81**, 1231–1240, doi:10.1175/1520-0477(2000)081<1231:TATCFS>2.3.CO;2.

Sippel, J. A., S. A. Braun, and C.-L. Shie, 2011: Environmental influences on the strength of Tropical Storm Debby (2006). *J. Atmos. Sci.*, **68**, 2557–2581, doi:10.1175/2011JAS3648.1.

Tallapragada, V., and Coauthors, 2012: Operational implementation of high-resolution triple-nested HWRF at NCEP/EMC—A major step towards addressing intensity forecast problem. *Proc. 30th Conf. on Hurricanes and Tropical Meteorology*, Ponte Verde, FL, Amer. Meteor. Soc., 14A.2. [Available online at https://ams.confex.com/ams/30Hurricane/webprogram/Paper205287.html.].

——, C. Kieu, Y. Kwon, S. Trahan, Q. Liu, Z. Zhang, and I.-H. Kwon, 2014: Evaluation of storm structure from the operational HWRF during 2012 implementation. *Mon. Wea. Rev.*, **142**, 4308–4325, doi:10.1175/MWR-D-13-00010.1.

Tien, D. D., T. Ngo-Duc, H. T. Mai, and C. Q. Kieu, 2013: A study of connection between tropical cyclone track and intensity errors in the WRF Model. *Meteor. Atmos. Phys.*, **122**, 55–64, doi:10.1007/s00703-013-0278-0.

Tien, T. T., C. Thanh, H. T. Van, and C. Q. Kieu, 2012: Two-dimensional retrieval of typhoon tracks from an ensemble of multimodel outputs. *Wea. Forecasting*, **27**, 451–461, doi:10.1175/WAF-D-11-00068.1.

Torn, R. D., and C. Snyder, 2012: Uncertainty of tropical cyclone best-track information. *Wea. Forecasting*, **27**, 715–729, doi:10.1175/WAF-D-11-00085.1.

Velden, C., and Coauthors, 2006: The Dvorak tropical cyclone intensity estimation technique: A satellite-based method that has endured for over 30 years. *Bull. Amer. Meteor. Soc.*, **87**, 1195–1210, doi:10.1175/BAMS-87-9-1195.

Ventham, J. D., and B. Wang, 2007: Large-scale flow patterns and their influence on the intensification rates of western North Pacific tropical storms. *Mon. Wea. Rev.*, **135**, 1110–1127, doi:10.1175/MWR3327.1.

Vukicevic, T., A. Aksoy, P. Reasor, S. D. Aberson, K. J. Sellwood, and F. Marks, 2013: Joint impact of forecast tendency and state error biases in ensemble Kalman filter data assimilation of inner-core tropical cyclone observations. *Mon. Wea. Rev.*, **141**, 2992–3006, doi:10.1175/MWR-D-12-00211.1.

Wu, C.-C., T.-S. Huang, W.-P. Huang, and K.-H. Chou, 2003: A new look at the binary interaction: Potential vorticity diagnosis of the unusual southward movement of Tropical Storm Bopha (2000) and its interaction with Super Typhoon Saomai (2000). *Mon. Wea. Rev.*, **131**, 1289–1300, doi:10.1175/1520-0493(2003)131<1289:ANLATB>2.0.CO;2.

Yablonsky, R. M., I. Ginis, B. Thomas, V. Tallapragada, D. Sheinin, and L. Bernardet, 2015: Description and analysis of the ocean component of NOAA's Operational Hurricane Weather Research and Forecasting Model (HWRF). *J. Atmos. Oceanic Technol.*, **32**, 144–163, doi:10.1175/JTECH-D-14-00063.1.

Zeng, Z., Y. Wang, and C.-C. Wu, 2007: Environmental dynamical control of tropical cyclone intensity—An observational study. *Mon. Wea. Rev.*, **135**, 38–59, doi:10.1175/MWR3278.1.